

This document is confidential and is proprietary to the American Chemical Society and its authors. Do not copy or disclose without written permission. If you have received this item in error, notify the sender and delete all copies.

**Dendrimer-Peptide Conjugates for Effective Blockade of the  
Interactions between SARS-CoV-2 Spike Protein and Human  
ACE2 Receptor**

Journal:	<i>Biomacromolecules</i>
Manuscript ID	bm-2022-01018d.R3
Manuscript Type:	Article
Date Submitted by the Author:	n/a
Complete List of Authors:	Jeong, Woo-jin; Inha University, Bu, Jiyoon; Inha University Mickel, Philip; University of Illinois Chicago Han, Yanxiao; University of Illinois at Chicago, Chemistry M/C 111 Rawding, Piper; University of Wisconsin Madison, Pharmaceutical Sciences Wang, Jianxin; University of Wisconsin Madison, Pharmaceutical Sciences Kang, Hanbit; Inha University Hong, Heejoo; Asan Medical Center Král, Petr; University of Illinois at Chicago, Chemistry M/C 111 Hong, Seungpyo; University of Wisconsin Madison, Pharmaceutical Sciences

**SCHOLARONE™**  
**Manuscripts**

1  
2  
3  
4  
5  
6  
7 Dendrimer-Peptide Conjugates for Effective  
8  
9  
10 Blockade of the Interactions between SARS-CoV-2  
11  
12  
13  
14  
15 Spike Protein and Human ACE2 Receptor  
16  
17  
18  
19  
20  
21  
22  
23  
24  
25  
26  
27  
28  
29  
30  
31  
32  
33  
34  
35  
36  
37  
38  
39  
40  
41  
42  
43  
44  
45  
46  
47  
48  
49  
50  
51  
52  
53  
54  
55  
56  
57  
58  
59  
60

# Dendrimer-Peptide Conjugates for Effective Blockade of the Interactions between SARS-CoV-2 Spike Protein and Human ACE2 Receptor

Woo-jin Jeong<sup>1,2,3†</sup>, Jiyoob Bu<sup>1,2,3‡</sup>, Philip Mickel<sup>4</sup>, Yanxiao Han<sup>4</sup>, Piper A Rawding<sup>1,2</sup>, Jianxin Wang<sup>2</sup>, Hanbit Kang<sup>3</sup>, Heejoo Hong<sup>5\*</sup>, Petr Králik<sup>4,6,7\*</sup>, and Seungpyo Hong<sup>1,2,8,9,10\*</sup>

<sup>1</sup>Pharmaceutical Sciences Division, The University of Wisconsin-Madison, 777 Highland Ave., Madison, WI 53705, USA

<sup>2</sup>Wisconsin Center for NanoBioSystems, The University of Wisconsin-Madison, 777 Highland Ave., Madison, WI 53705, USA

<sup>3</sup>Department of Biological Sciences and Bioengineering, Inha University, 100 Inha-ro, Michuhol-gu, Incheon 22212, KOREA

<sup>4</sup>Department of Chemistry, University of Illinois at Chicago, Chicago, IL 60607, USA

<sup>5</sup>Department of Clinical Pharmacology & Therapeutics, Asan Medical Center, University of Ulsan, 88 Olympic-ro 43-gil, Songpa-gu, Seoul 05505, KOREA

<sup>6</sup>Department of Physics, University of Illinois at Chicago, Chicago, IL 60607, USA

<sup>7</sup>Department of Pharmaceutical Sciences, University of Illinois at Chicago, Chicago, IL 60612, USA

<sup>8</sup>Lachman Institute for Pharmaceutical Development, The University of Wisconsin-Madison, 777 Highland Ave., Madison, WI 53705, USA

1  
2  
3     <sup>9</sup>Yonsei Frontier Lab and Department of Pharmacy, Yonsei University, Seoul 03722, KOREA  
4  
5  
6     \*Co-corresponding authors  
7  
8     <sup>‡</sup>Both authors contributed equally.  
9  
10  
11  
12  
13

14     ABSTRACT. The coronavirus disease 2019 (COVID-19) pandemic has threatened the stability of  
15     global healthcare, which is becoming an endemic issue. Despite the development of various  
16  
17     treatment strategies to fight COVID-19, the currently available treatment options showed varied  
18  
19     efficacy. Herein, we have developed an avidity-based SARS-CoV-2 antagonist using dendrimer-  
20  
21     peptide conjugates (DPCs) for effective COVID-19 treatment. Two different peptide fragments  
22  
23     obtained from angiotensin-converting enzyme 2 (ACE2) were integrated into a single sequence,  
24  
25     followed by the conjugation to poly(amidoamine) (PAMAM) dendrimers. We hypothesized that  
26  
27     the strong multivalent binding avidity endowed by dendrimers would help peptides effectively  
28  
29     block the interaction between SARS-CoV-2 and ACE2, and this antagonist effect would be  
30  
31     dependent upon the generation (size) of the dendrimers. To assess this, binding kinetics of the  
32  
33     DPCs prepared from generation 4 (G4) and G7 PAMAM dendrimers to spike protein of SARS-  
34  
35     CoV-2 were quantitatively measured using surface plasmon resonance. The larger dendrimer-  
36  
37     based DPCs exhibited significantly enhanced binding strength by three orders of magnitude  
38  
39  
40  
41  
42  
43  
44  
45  
46  
47  
48  
49  
50  
51  
52  
53  
54  
55  
56  
57  
58  
59  
60

1  
2  
3 compared to the free peptides, whereas the smaller one showed a 12.8-fold increase only. An *in*  
4  
5 *vitro* assay using SARS-CoV-2-mimicking microbeads also showed the improved SARS-CoV-2  
6  
7 blockade efficiency of the G7-peptide conjugates compared to G4. In addition, the interaction  
8  
9 between the DPCs and SARS-CoV-2 was analyzed using molecular dynamics (MD) simulation,  
10  
11 providing an insight of how dendrimer-mediated multivalent binding effect can enhance the  
12  
13 SARS-CoV-2 blockade. Our findings demonstrate that the DPCs having strong binding to SARS-  
14  
15 CoV-2 effectively blocks the interaction between ACE2 and SARS-CoV-2, providing a potential  
16  
17 as a high-affinity drug delivery system to direct anti-COVID payloads to the virus.  
18  
19  
20  
21  
22  
23  
24  
25  
26  
27  
28  
29  
30  
31  
32 **KEYWORDS.** COVID-19, SARS-CoV-2, Dendrimer-peptide conjugates, Multivalent binding,  
33  
34  
35 Avidity, Molecular dynamics  
36  
37  
38  
39  
40 **INTRODUCTION**  
41  
42  
43  
44 Increasing changes in our society and environment have resulted in the emergence of novel and  
45  
46 modified pathogens, resulting in significant global health challenges.<sup>1</sup> One such family of the  
47  
48 emerging pathogens is Coronavirus (CoV) that is characterized by its high prevalence and  
49  
50 distribution, genetic diversity, and rapid evolution.<sup>2</sup> Since the 1970s, a series of CoV infections  
51  
52  
53  
54  
55  
56  
57  
58  
59  
60

1 have been reported in domestic animals;<sup>3</sup> however, they were not considered highly pathogenic to  
2

3 humans until the outbreak of severe acute respiratory syndrome (SARS) in the early 2000s in China  
4

5 and Middle East respiratory syndrome (MERS) in the early 2010s in Middle Eastern countries.<sup>4,5</sup>  
6

7 In late December 2019, a new CoV infection, SARS-CoV-2, emerged in China and named  
8

9 coronavirus disease (COVID-19).<sup>2,6</sup> SARS-CoV-2 is an enveloped, positive-sense, and single-  
10

11 stranded RNA (+ssRNA) virus that belongs to the group of  $\beta$ -coronavirus ( $\beta$ -CoV), similar to both  
12

13 SARS and MERS; these viruses can infect mammals and jump species barriers, resulting in  
14

15 animal-to-human transmission. A full-length genome sequence has revealed that the SARS-CoV-  
16

17 2 is closely related with the other  $\beta$ -COV members, sharing ~80% and ~50% sequence identities  
18

19 with SARS-CoV-1 and MERS-CoV, respectively.<sup>7</sup> Whereas the clinical features of COVID-19  
20

21 patients were described shortly after the emergence of the disease, no effective treatment was  
22

23 available. As a result, the World Health Organization (WHO) declared COVID-19 a global  
24

25 pandemic due to its high transmissibility and severity.<sup>8-10</sup> Since the beginning of the pandemic,  
26

27 mitigation strategies have included social distancing, wearing facemasks, travel restrictions, stay-  
28

29 at-home orders, and viral testing. With the successful development, evaluation, and production of  
30

31 multiple vaccines, however, vaccination has helped reduce the widespread of COVID-19.<sup>11</sup>  
32

1  
2  
3 However, as of 20 January 2022, there have been 5.57 million confirmed deaths and 342 million  
4  
5 confirmed cases of infection with SARS-CoV-2.<sup>12</sup>  
6  
7

8  
9  
10 Various treatment strategies have emerged with the appearance of COVID-19, including  
11  
12 drug-based conventional approaches, peptides,<sup>13,14</sup> sulfonated glyco-dendrimers,<sup>15</sup> monoclonal  
13  
14 antibodies, plasma therapy, and mechanical ventilation.<sup>16</sup> Amongst drug-based treatment  
15  
16 strategies, the nucleoside analog prodrug Remdesivir (GS-5734) has received much attention due  
17  
18 to its remarkable antiviral effect for SARS-CoV-1 and MERS-CoV in pre-clinical trials and animal  
19  
20 studies.<sup>17,18</sup> However, recent clinical results obtained from a large cohort of 330 patients in 30  
21  
22 different countries suggest that the drug appears to have no significant effect on COVID-19  
23  
24 mortality, contradicting previous findings.<sup>19</sup> Alternatively, oral antiviral drugs such as Paxlovid  
25  
26 (nirmatrelvir/ritonavir) and Molnupiravir (Lagevrio) have been authorized for preventing mild to  
27  
28 moderate COVID-19 from worsening. However, these oral medications interact badly with other  
29  
30 concurrent medications which have the potential to cause serious adverse effects, such as impaired  
31  
32 taste and high blood pressure.<sup>20</sup>  
33  
34

35 Several monoclonal antibody treatments have also obtained clinical attention to combat  
36  
37 SARS-CoV-2.<sup>20</sup> SARS-CoV-2 utilizes spike glycoproteins (Spike proteins) on their envelope to  
38  
39

1  
2  
3 interact with angiotensin-converting enzyme 2 (ACE2) receptors present on lung tissue.<sup>21-24</sup> The  
4  
5 binding of Spike proteins to ACE2 receptors is recognized as the most critical step for the SARS-  
6  
7 CoV-2 infection, promoting viral cell entry.<sup>25-27</sup> Most of the currently available monoclonal  
8  
9 antibody medications, such as Bamlanivimab (LY-CoV555) and a combination of Casirivimab  
10  
11 (REGN10933)/Imdevimab (REGN10987), prevent the interaction between the Spike protein and  
12  
13 ACE2 receptors via blockade of the receptor-binding domain (RBD) on the spike protein.<sup>28-31</sup>  
14  
15  
16  
17 Although these antibody drugs also received EUA from the FDA to treat mild-to-moderate  
18  
19 COVID-19 patients,<sup>32</sup> their clinical benefits remain unclear to the hospitalized patients.<sup>33</sup> Given  
20  
21 that the currently available COVID-19 treatments are of varied efficacy, more focus is on the  
22  
23 prevention of transmission through vaccination rather than the treatment of the virus itself.<sup>34</sup> Thus,  
24  
25  
26 there is a significant need for an effective treatment for COVID-19 patients.  
27  
28  
29  
30  
31  
32  
33  
34  
35  
36  
37  
38  
39  
40  
41 Early modeling and experiments have revealed that individual ACE2-based peptides can  
42  
43 efficiently bind to the Spike proteins of SARS-CoV-2.<sup>13-15</sup> For example, Pomplun et al. identified  
44  
45 three peptide sequences that form high-affinity binding with RBD on the Spike proteins<sup>35</sup>. These  
46  
47 peptides demonstrated high selectivity towards SARS-CoV-2-spike-RBD, demonstrating a  
48  
49 potential use of peptides as a target molecule for SarS-CoV-2. Herein, we examined the use of  
50  
51  
52  
53  
54  
55  
56  
57  
58  
59  
60

1  
2  
3 engineered dendrimer-peptide conjugates (DPCs) for COVID-19 treatment. Previously, DPCs  
4  
5 have demonstrated potent protein–protein interaction (PPI) inhibitory functions, high target  
6  
7 affinity and selectivity, and enhanced bioavailability or pharmacokinetics compared to the free  
8  
9 peptides.<sup>36–38</sup> Considering that S proteins form trimers and bind to ACE2 protein via multivalent  
10  
11 binding, the utilization of DPCs for COVID-19 treatment can be a promising strategy to develop  
12  
13 strong inhibitors of S protein binding to ACE2 receptors. In this study, two peptide fragments of  
14  
15 ACE2 were incorporated into a single sequence and conjugated to the surface of poly(amidoamine)  
16  
17 (PAMAM) dendrimers, based on the assumption that the multivalent ACE2-mimicking peptides  
18  
19 could effectively block the S protein-ACE2 interaction (**Figure 1**). We investigated the therapeutic  
20  
21 potential of DPC approach by exploring its S protein-ACE2 interaction with conventional  
22  
23 antibodies. Further, we provide a resource for designing efficacious and cost-effective DPC-based  
24  
25 SARS-CoV-2 target agents, which may have important implications for delivering antiviral  
26  
27 payloads to SARS-CoV-2 with high affinity and selectivity.  
28  
29  
30  
31  
32  
33  
34  
35  
36  
37  
38  
39  
40  
41  
42  
43  
44  
45  
46  
47  
48  
49  
50  
51  
52  
53  
54  
55  
56  
57  
58  
59  
60

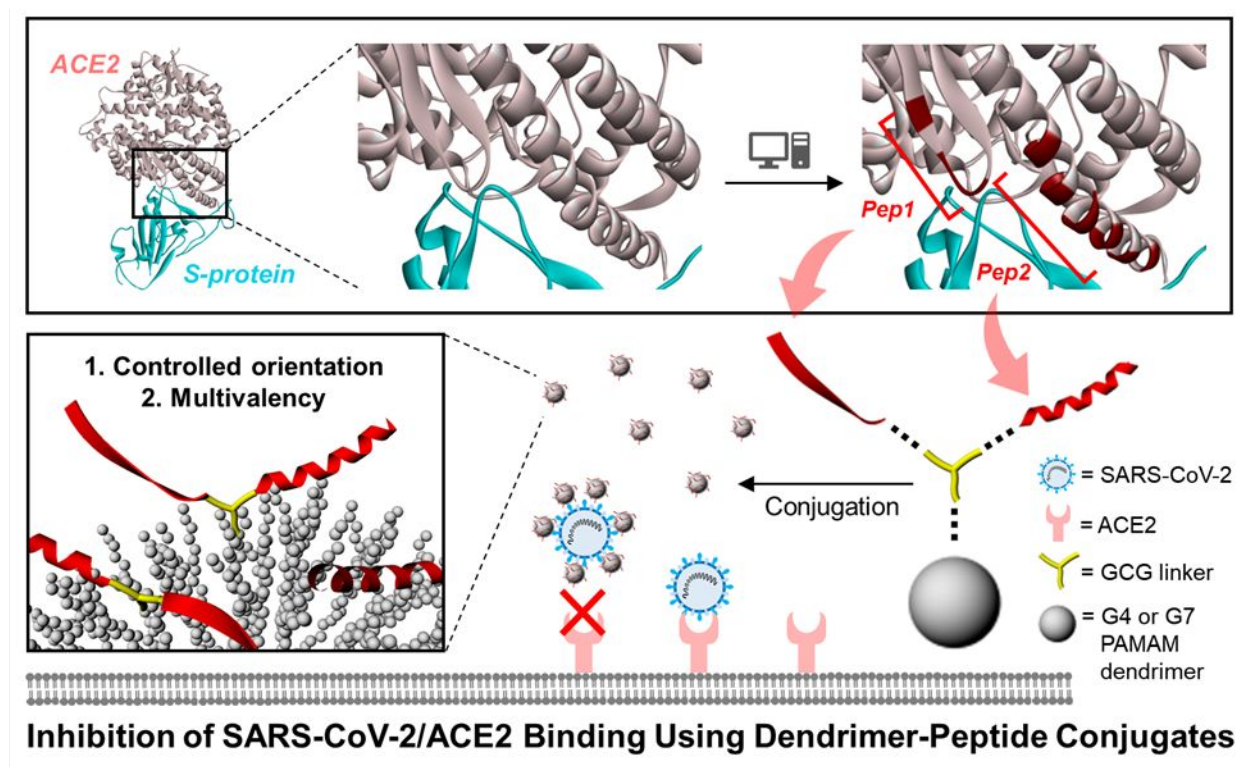


Figure 1. Inhibition of SARS-CoV-2/ACE2 (PDB ID: 2AJF) binding using dendrimer-peptide conjugates consisting of two peptides, a linker, and a dendrimer.

## EXPERIMENTAL SECTION

**Cell culture.** Two human breast cancer cell lines, MDA-MB-231 and MCF-7, were used in this study. MDA-MB-231 and MCF-7 cells were cultured in Leibovitz's L-15 medium Dulbecco's modified eagle medium (DMEM), respectively, supplemented with 10% (v/v) FBS and 1% (v/v)

1  
2  
3 P/S. Cells were cultured in a controlled humidified atmosphere with 5% CO<sub>2</sub> at 37 °C and grown  
4  
5  
6 in T-25 flasks until they reach 60-80% confluence.  
7  
8  
9

10  
11 **Bead preparation.** The bead binding assay was performed to assess the blockade of S protein for  
12  
13 each inhibitor. The carboxyl groups on fluorescently labelled beads (Bang laboratories; 2 × 10<sup>6</sup>  
14  
15 beads in 1 mL PBS) were activated using 1.8 mg/mL 1-(3-Dimethylaminopropyl)-3-  
16  
17 EthylcarbodiimideHydrochloride (EDC) and 2.8 mg/mL N-Hydroxy-Succinimide (NHS) (Sigma-  
18  
19 Aldrich, St. Louis, MO). After 20 min EDC/NHS treatment, the beads were centrifuged for 3 min  
20  
21 at 5,000g. Followed by 2 h incubation with 0.5 mg 5,000 MW carboxy-polyethylene glycol-amine  
22  
23 (PEG; Nektar Therapeutics, Huntsville, AL). Unimmobilized PEG were then removed from the  
24  
25 PEGylated beads using centrifugation (3 min, 5,000g, three times). PEGylated beads were  
26  
27 functionalized with 5 µg/mL S protein using the same EDC/NHS chemistry. S protein-immobilized  
28  
29 beads were then incubated with bovine serum albumin for 3 h to block the non-specific bindings.  
30  
31  
32  
33  
34  
35  
36  
37  
38  
39  
40  
41  
42  
43  
44  
45

46 ***In vitro* bead binding assay.** Cells were incubated in a 96-well plate and grown until they reach  
47  
48 80% confluence. The S protein-immobilized beads were incubated with different inhibitors for 30  
49  
50 min including free pACE2 peptides, the G4-pACE2 conjugates, the G7-pACE2 conjugates, and  
51  
52 anti-SARS-CoV-2 antibodies, and each inhibitor was treated to the cells for 1 h in a serum-free  
53  
54  
55  
56  
57  
58  
59  
60

1  
2  
3 media at the concentration of  $10^4$  particles per well in a 96-well plate. The number of beads bound  
4  
5 to the cell surface was counted after three times of PBS washing.  
6  
7  
8  
9  
10

11 **Molecular dynamics simulation.** The systems were simulated using NAMD 2.13<sup>34,35</sup> and the  
12 CHARMM36<sup>36-38</sup> protein force field. The simulations were conducted with the Langevin  
13  
14 dynamics ( $\gamma_{ang} = 1 \text{ ps}^{-1}$ ) in the NpT ensemble, at a temperature of  $T = 310 \text{ K}$  and a pressure of  $p =$   
15  
16  
17  
18 1 bar. The particle-mesh Ewald (PME) method was used to evaluate Coulomb coupling, with  
19  
20 periodic boundary conditions applied.<sup>44</sup> The time step was set to 2 fs. The long-range van der  
21  
22 Waals and Coulombic coupling were evaluated every 1- and 2-time steps, respectively. After  
23  
24  
25 200,000 steps of minimization, the solvent molecules were equilibrated for 4 ns, while the  
26  
27  
28 dendrimers and RBD were constrained using harmonic forces with a spring constant of 1 kcal (mol  
29  
30  
31 Å)<sup>-1</sup>. Next, the systems were equilibrated in for 100 ns with the bottom residues on the S protein  
32  
33  
34 RBD constrained.  
35  
36  
37  
38  
39  
40  
41  
42  
43  
44  
45

46 **MMGB-SA calculations:** The molecular mechanics generalized Born-surface area (MMGB-SA)  
47  
48 method<sup>14,40,41</sup> was used to estimate the free energies of binding between peptides and RBDs. The  
49  
50 free energies were estimated from separate MMGB-SA calculations for three systems (binding  
51  
52 amino acids, RBD, and the whole complex) in configurations extracted from the MD trajectories  
53  
54  
55  
56  
57  
58  
59  
60

of the whole complex in the explicit solvent. The MMGB-SA free energies of the extracted configurations of the systems were calculated as

$$G_{tot} = E_{MM} + G_{solv-p} + G_{solv-np} - T\Delta S_{conf} \quad (1)$$

where  $E_{MM}$ ,  $G_{solv-p}$ ,  $G_{solv-np}$ , and  $T\Delta S_{conf}$  are the sum of bonded and Lennard-Jones energy terms, the polar contribution to the solvation energy, the nonpolar contribution, and the conformational entropy, respectively. The  $E_{MM}$ ,  $G_{solv-p}$ , and  $G_{solv-np}$  terms were calculated using the NAMD 2.13<sup>34,35</sup> package generalized Born implicit solvent model,<sup>42</sup> with the dielectric constant of water  $\epsilon = 78.5$ . The  $G_{solv-np}$  term for each system configuration was calculated in NAMD as a linear function of the solvent-accessible surface area (SASA), determined using a probe radius of 1.4 Å, as  $G_{solv-np} = \gamma_{SASA}$ , where  $\gamma = 0.00542 \text{ kcal mol}^{-1} \text{ Å}^{-2}$  is the surface tension. The  $\Delta S_{conf}$  term was neglected since the entropic contribution nearly cancels when considering protein-protein binding of such similar structures. Since the  $G_{tot}$  values are obtained for peptide configurations extracted from the trajectories of complexes,  $G_{tot}$  does not include the free energies of peptide reorganization; the correct free energies of binding should consider configurations of separately

1  
2  
3 relaxed systems. The approximate binding free energies of the studied complexes were calculated  
4  
5  
6 as:  
7  
8  
9  
10  
11  
12

$$\langle \Delta G_{MMGB-SA} \rangle = \langle G_{tot}(\text{peptides} - \text{RBD}) - G_{tot}(\text{peptides}) - G_{tot}(\text{RBD}) \rangle \quad (2)$$

20 where peptides represent the chosen binding peptides, and the  $\langle \text{averaging} \rangle$  is performed over  
21  
22 configurations within the last 50 ns of the calculated trajectories.  
23  
24  
25  
26  
27

28 **RMSD calculations:** Time-dependent RMSD for the pACE2-1, pACE2-2, and pACE2-3  
29  
30 conjugated dendrimers were calculated from  
31  
32  
33  
34  
35  
36  
37  
38

$$RMSD_{\alpha}(t_j) = \sqrt{\frac{\sum_{\alpha=1}^{N_{\alpha}} (\vec{r}_{\alpha}(t_j) - \vec{r}_{\alpha}(t_0))^2}{N_{\alpha}}} \quad (3)$$

39  
40  
41  
42  
43  
44  
45  
46 where  $N_{\alpha}$  is the number of atoms whose positions are being compared,  $\vec{r}_{\alpha}(t_j)$  is the position of  
47  
48 atom  $\alpha$  at time  $t_j$  and  $\vec{r}_{\alpha}(t_0)$  is the initial coordinate.<sup>43</sup> The time-dependent RMSD was averaged  
49  
50 over the last 50 ns of simulation time and is shown in Figure 5.  
51  
52  
53  
54  
55  
56  
57  
58  
59  
60

1  
2  
3  
4  
5  
6  
7  
8  
9  
10  
11  
12  
13  
14  
15  
16  
17  
18  
19  
20  
21  
22  
23  
24  
25  
26  
27  
28  
29  
30  
31  
32  
33  
34  
35  
36  
37  
38  
39  
40  
41  
42  
43  
44  
45  
46  
47  
48  
49  
50  
51  
52  
53  
54  
55  
56  
57  
58  
59  
60

## RESULTS AND DISCUSSION

In our previous study, it was found that the 15 amino acid residues of ACE2 play critical role in the S protein binding.<sup>13</sup> Hence, considering that 13 of the residues are included in two short peptide fragments (KGDFR and DKFNHEAEDLFYQ) that are closely located in a small area (Figure 2a), we designed and synthesized a S protein-binding peptide (pACE2) composed of the two sequences and a short linker. A cysteine residue was introduced in the middle of the linker and used for the dendrimer conjugation, which allowed mimicking of spatial positions and orientations of the two peptide fragments in the ACE2 structure, as demonstrated in a previous study (Figure 2b). Therefore, the conjugation to the dendrimer surface enabled the peptides not only to form multivalent binding with S proteins but also to mimic the active site of ACE2, which could significantly enhance their target binding affinity as demonstrated in previous studies.<sup>49-51</sup>

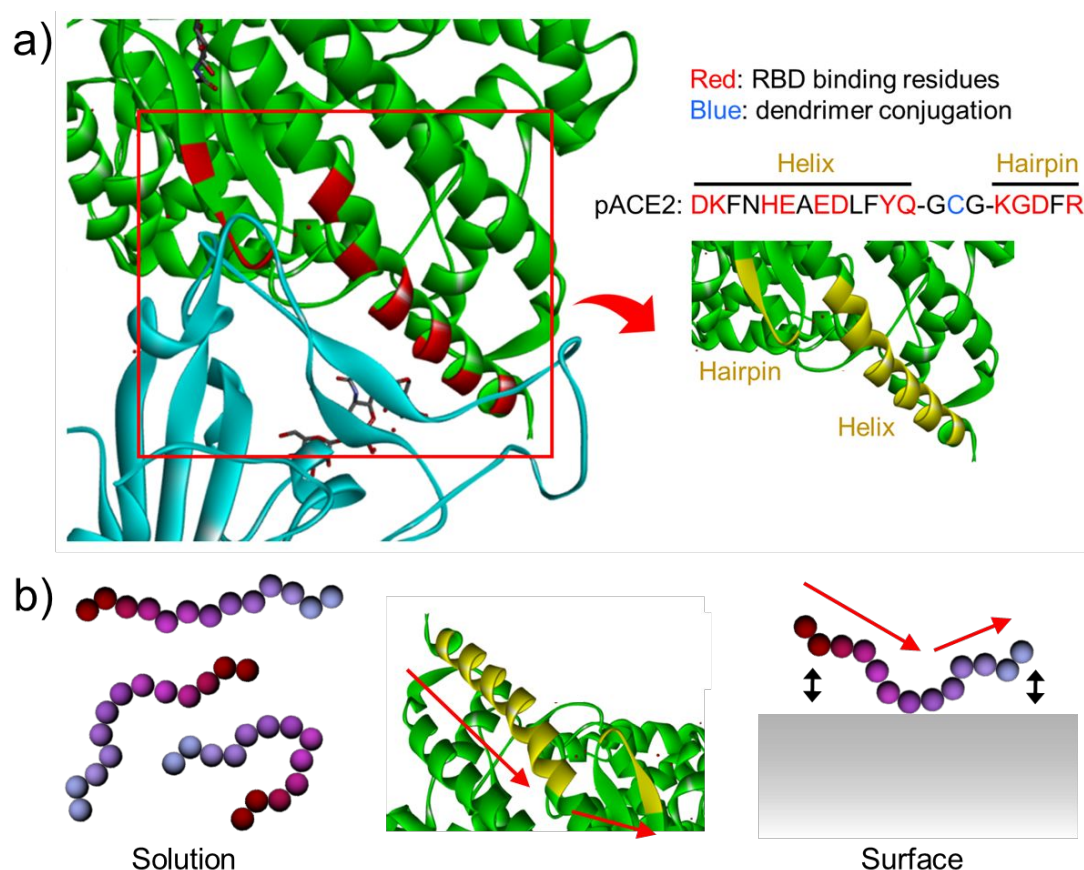


**Figure 2.** (a) The structure of synthesized S protein-binding peptide (pACE2) composed of the two sequences and a short linker. (b) Schematic illustration of the surface conjugation-mediated mimicry of molecular configuration of the ACE2 active site.

SARS-CoV-2 spike protein-targeting dendrimer nanoparticles were prepared by the conjugation of approximately 4 and 40 pACE2 peptides to G4 (G4-pACE2 conjugates) and G7 PAMAM dendrimers (G7-pACE2 conjugates), respectively (Figure S2, S3, S4, and S5). Note that the number of peptides conjugated to each generation of dendrimers was determined to be less

1  
2  
3 than 10% of the total primary amine groups. This would provide sufficient distance between the  
4  
5 ligands and enable effective binding with the target molecules, as described previously.<sup>49</sup> Surface  
6  
7 plasmon resonance (SPR) analysis indicated that the dendrimer-pACE2 conjugates bind more  
8  
9 strongly with spike proteins than the free pACE2 peptides (Figure 3). The G4-pACE2 conjugates  
10  
11 bound to spike proteins with a dissociation constant ( $K_D$ ) of  $1.84 \times 10^{-1}$   $\mu\text{M}$  which was 12.8-fold  
12  
13 smaller than the  $K_D$  of free pACE2 peptides with spike proteins (2.35  $\mu\text{M}$ ). The increase in binding  
14  
15 avidity was more prominent when pACE2 peptides were conjugated to the G7 PAMAM  
16  
17 dendrimers. The binding avidity of the G7-pACE2 conjugates for spike proteins was three orders  
18  
19 of magnitude stronger ( $K_D = 5.04 \times 10^{-3}$   $\mu\text{M}$ ) than the free pACE2 peptides. On the other hand,  
20  
21 the scrambled pACE2 peptides (pACE2\_SC), G4-pACE2\_SC, and G7-pACE2\_SC showed little-  
22  
23 to-no binding to the spike proteins (Figure S6). Specifically, a direct comparison of SPR  
24  
25 sensograms revealed that the smaller  $K_D$  of the G7-pACE2 conjugates compared to that of the G4-  
26  
27 pACE2 conjugates or free pACE2 peptides was attributed to both faster association and slower  
28  
29 dissociation with the target molecules. Surprisingly,  $K_D$  of the G7-pACE2 conjugates was  
30  
31 comparable to its whole antibody counterpart (anti-SARS-CoV-2 antibody) which binds to spike  
32  
33 proteins with  $K_D$  of  $2.07 \times 10^{-3}$   $\mu\text{M}$ . As circular dichroism (CD) analysis showed negligible  
34  
35  
36  
37  
38  
39  
40  
41  
42  
43  
44  
45  
46  
47  
48  
49  
50  
51  
52  
53  
54  
55  
56  
57  
58  
59  
60

conformational change in the peptides according to the conjugation (Figure S7), we speculated that the number of ligand molecules on the dendrimer surface highly affects the affinity to spike proteins that were densely packed on the SPR sensor chip. Also, considering that the trimeric spike protein is composed of three monomers with each having an RBD, the multivalent binding effect of the dendrimers enabled cooperative and strong interaction between RBD and pACE2 peptides, which eventually increased the binding avidity towards spike proteins.

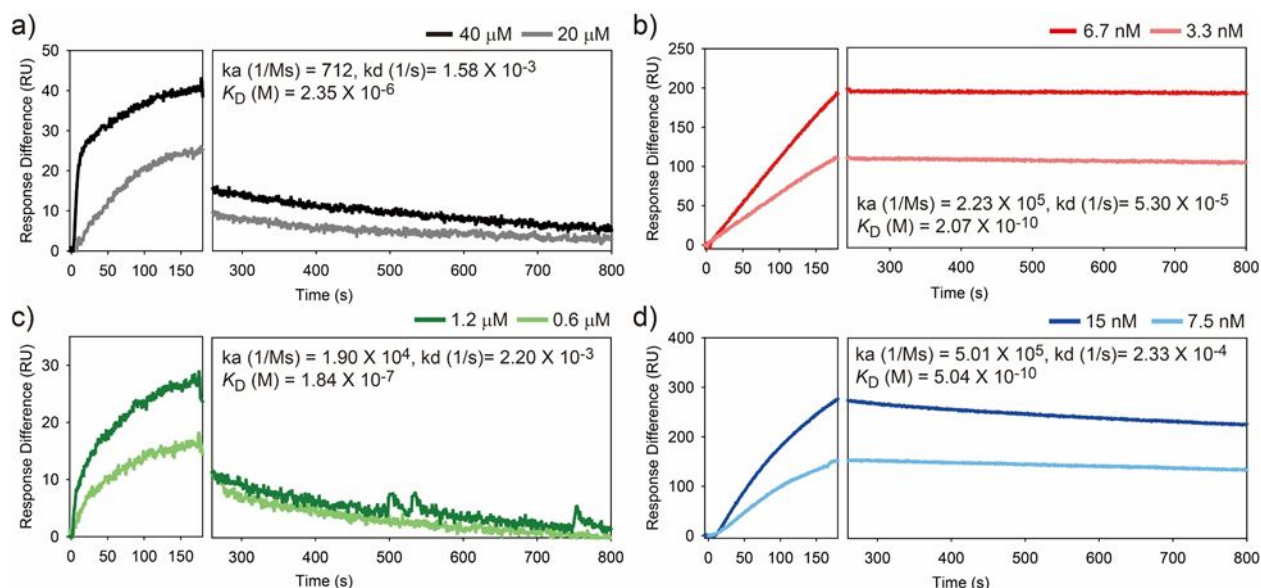


**Figure 3.** SPR sensorgrams for binding of (a) free pACE2, (b) anti-S protein antibody, (c) G4-pACE2, and (d) G7-pACE2 to S proteins.

1  
2  
3 The inhibition between the ACE2 and SARS-CoV-2 spike proteins was then assessed *in*  
4  
5  
6 *vitro* using spike protein-coated fluorescent beads as a representative model for SARS-CoV-2.  
7  
8

9  
10 Note that the size of the beads (10  $\mu$ m) was larger than the actual SARS-CoV-2 virus. The beads  
11  
12 were incubated with different inhibitors for 30 min including free pACE2 peptides, the G4-pACE2  
13  
14 conjugates, the G7-pACE2 conjugates, and anti-SARS-CoV-2 antibodies, and each inhibitor was  
15  
16 treated to the cells for 1 h in a serum-free media at the concentration of  $10^4$  particles per well in a  
17  
18 96-well plate. As demonstrated in **Figure 4**, the G4-pACE2 conjugates effectively inhibited the  
19  
20 interaction between the spike protein-coated beads and ACE2-expressing MCF-7 cells, resulting  
21  
22 in a ~39.3% reduced bead binding compared to the beads without any inhibitor treatment ( $p =$   
23  
24 0.047). This was even more pronounced for the G7-pACE2 conjugates which showed an ~51.4%  
25  
26 reduced bead binding on MCF-7 cells ( $p = 0.028$ ). In contrast, the free pACE2 peptides did not  
27  
28 induce a noticeable difference with the non-treated controls, which implies that the inhibitory  
29  
30 effect of the dendrimer-PACE2 conjugates is attributed to the enhanced binding kinetics of the  
31  
32 conjugates to SARS-CoV-2 spike protein. However, the dendrimer-pACE2 conjugates were less  
33  
34 effective than the anti-SARS-CoV-2 antibodies which demonstrated ~73.3% reduction in bead  
35  
36 binding, although the results were statistically insignificant ( $p = 0.255$  for the G7-pACE2  
37  
38  
39  
40  
41  
42  
43  
44  
45  
46  
47  
48  
49  
50  
51  
52  
53  
54  
55  
56  
57  
58  
59  
60

1  
2  
3 conjugates vs. anti-SARS-CoV-2 antibodies). This was contradictory to the results obtained from  
4  
5 the SPR assay, as the G7-pACE2 conjugates were expected to exhibit a similar level of *in vitro*  
6  
7 inhibitory effect to the antibodies. The lower *in vitro* efficiency of the G7-pACE2 conjugates  
8  
9 compared to the SARS-CoV-2 antibodies is presumably due to the structural difference between  
10  
11 the spike proteins on an actual virus and the microbead surface. The spike proteins on SARS-  
12  
13 CoV-2 are comprised of a trimetric structure, while this structure is not maintained on the bead  
14  
15 surface. Considering that the multivalent binding effect of the dendrimers would be more effective  
16  
17 on trimetric structure, the dendrimer-pACE2 conjugates are expected to have a stronger inhibitory  
18  
19 effect on an actual virus. It should be also noted that the free dendrimers or S protein beads without  
20  
21 any inhibitor treatment did not induce a noticeable inhibitory effect on cells. Furthermore, the  
22  
23 inhibitors used in this study had a minor effect on MDA-MB-231 cells which have low ACE2  
24  
25 expressions, demonstrating the selectivity of our dendrimer-pACE2 conjugates for targeting the  
26  
27 spike proteins.  
28  
29  
30  
31  
32  
33  
34  
35  
36  
37  
38  
39  
40  
41  
42  
43  
44  
45  
46  
47  
48  
49  
50  
51  
52  
53  
54  
55  
56  
57  
58  
59  
60

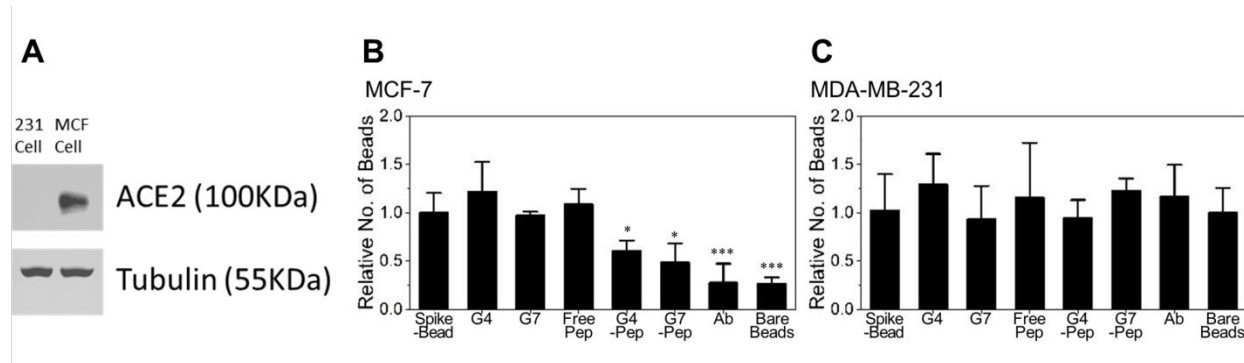


**Figure 4.** The inhibition between the ACE2 and SARS-CoV-2 spike proteins assessed *in vitro* using spike protein-coated fluorescent beads as a representative model for SARS-CoV-2. (a) Western blot analysis demonstrating the expression levels of ACE2 protein in MCF-7 and MDA-MB-231 cells. (b, c) The binding of spike protein-coated beads on MCF-7 and MDA-MB-231 cells after incubating the beads with either G4, G7, free pACE2, G4-pACE2, G7-pACE2, or antibodies for 1 h. Note that the statistical significance was analyzed compared to S protein-conjugated beads without any inhibitor treatments. Significance levels are indicated as \* $p < 0.05$ , \*\* $p < 0.01$ , and \*\*\* $p < 0.001$ , which are analyzed using Student's *t*-test.

In this study, we have demonstrated that pACE2 peptides immobilized on PAMAM dendrimer surfaces block the binding of spike proteins to ACE proteins more effectively through

1  
2  
3 a multivalent binding effect. Compared to free pACE2 peptides (negative controls), a high-density  
4  
5 of reactive sites on the dendrimer surface allow for the conjugation of multiple peptides in a  
6  
7 controlled distance. The flexible three-dimensional molecular structure of the PAMAM  
8  
9 dendrimers then facilitates multiple interactions between peptides and spike proteins to occur in a  
10  
11 single nano-structure. Molecular dynamics (MD) simulations of the studied systems were  
12  
13 performed to better understand the experimental results, compare different dendrimer-peptide  
14  
15 systems, and examine the benefits of the dendrimer-mediated multivalent binding effect.<sup>13–15,52</sup> A  
16  
17 multivalent binding between peptide-conjugated dendrimers and the receptor binding domain  
18  
19 (RBD) of the Spike protein of SARS-CoV-2. Three peptides were tested for their binding to RBD:  
20  
21  
22 pACE2-1 (sequence DKFNHEAEDLFYQ-GCG-KGDFR), pACE2-2 (residues 22 to 88 in PDB  
23  
24 6M17, MET residue 88 mutated to CYS to link with sulfo-SMCC), and pACE2-3 (N-terminus and  
25  
26 C-terminus of pACE2-2 bonded together). Six pACE2-1 and three pACE2-2/pACE2-3 were  
27  
28 conjugated to a generation 4 PAMAM dendrimer via a sulfo-SMCC linker forming three  
29  
30 conjugated dendrimers (pACE2-1-dendrimer, pACE2-2-dendrimer, and pACE2-3-dendrimer).  
31  
32  
33 The three conjugated dendrimers were subsequently placed above the RBD with one of the  
34  
35 peptides binding to the RBD as in PDB 6M17. **Figures 5** shows typical binding configurations for  
36  
37  
38  
39  
40  
41  
42  
43  
44  
45  
46  
47  
48  
49  
50  
51  
52  
53  
54  
55  
56  
57  
58  
59  
60

the individual peptides after 100 ns long MD simulations. All peptides remained in or near the binding position over the entire simulation trajectory.

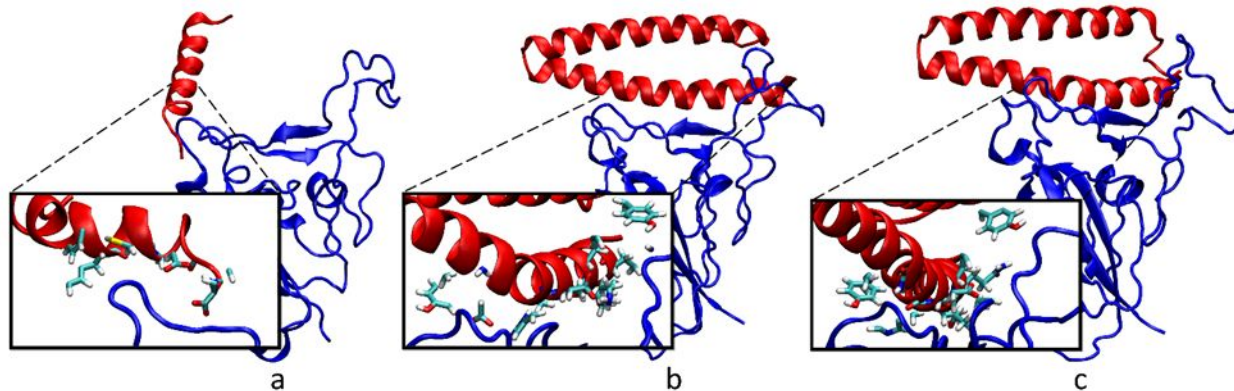


**Figure 5.** Binding of (a) pACE2-1, (b) pACE2-2, and (c) pACE2-3 free peptides to the RBD of the S protein of SARS-CoV-2. Red chains are the free peptides and blue chains are the RBD. Note that frames shown are 50 ns into the simulation.

**Figures 6a-c** show typical binding configurations for the three conjugated dendrimers after 125.8, 100.2, and 123.8 ns long MD simulations, respectively. Each of the three systems remained in a binding configuration throughout the whole simulation trajectory, where the peptides were close to their original configurations and conformations (folding). The peptides on the dendrimers also remained folded throughout the simulations, except pACE2-1. **Figures 6d and 6e** show the free energies of binding and RMSDs, respectively, of the isolated and dendrimer-attached peptides.

1  
2  
3 While pACE2-1 has a favorable free energy of binding, pACE2-2 and pACE2-3 have lower free  
4  
5 energies and as such larger affinity with the RBD. For pACE2-1, almost all the free energy is  
6  
7 derived from the binding peptides, which is not the case for pACE2-2 and pACE2-3. The  
8  
9 dendrimer and non-binding peptides contribute a sizeable amount to the free energy in both, likely  
10  
11 due to stabilization of the region binding with the RBD. We can also see that pACE2-1 has a higher  
12  
13 but comparable RMSD of its binding peptides, while conjugated, than that of pACE2-2 and  
14  
15 pACE2-3. All three proposed peptides have an average RMSD of less than 3 Å when binding with  
16  
17 the Spike protein RBD. However, the RMSD of the free peptides is much higher for pACE2-1  
18  
19 than either pACE2-2 or pACE2-3, suggesting that it does not remain consistently tightly bound  
20  
21  
22  
23  
24  
25  
26  
27  
28  
29  
30  
31  
32  
33  
34 with the RBD.

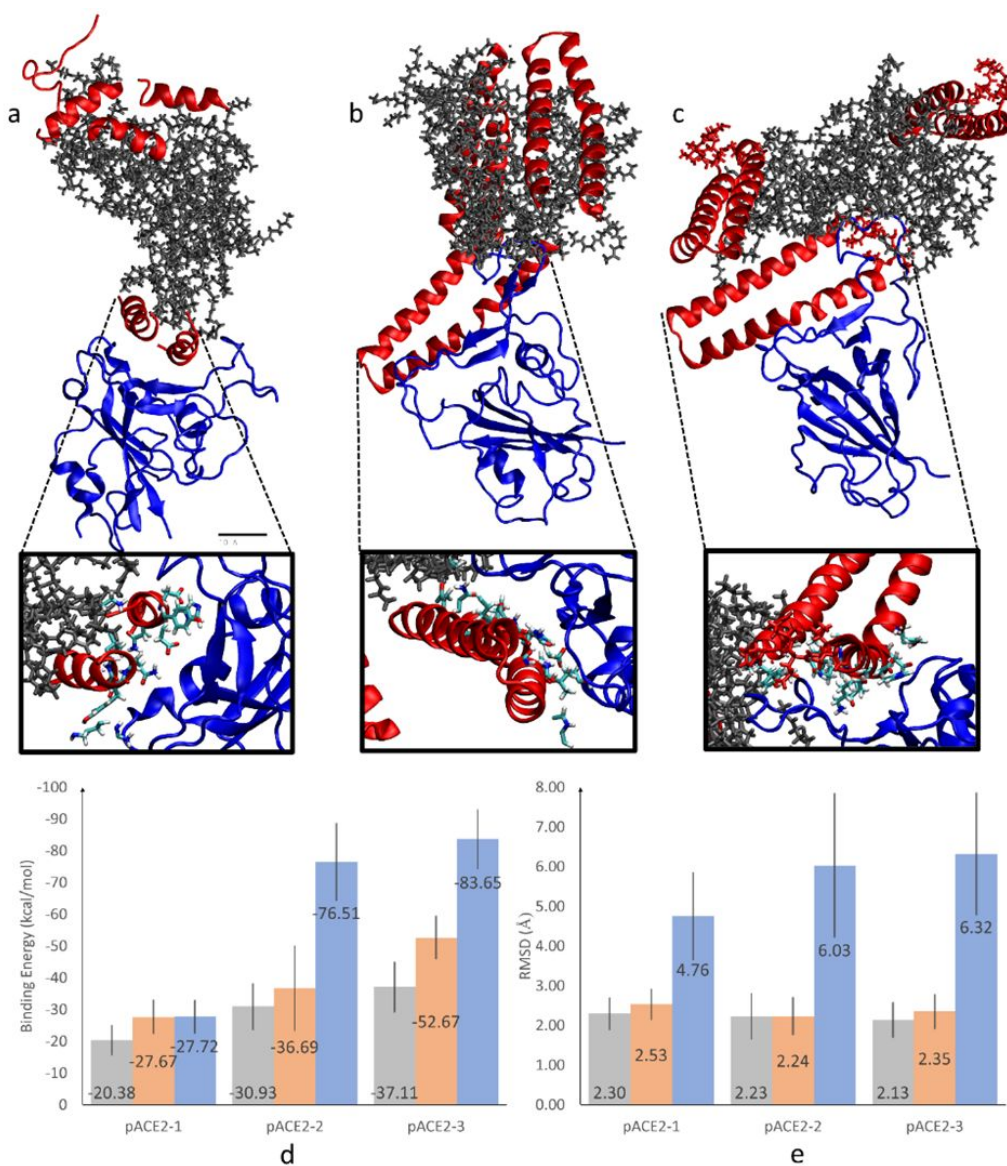


Figure 6. Binding of (a) pACE2-1, (b) pACE2-2, and (c) pACE2-3-conjugated generation 4

PAMAM dendrimers to the RBD of the S protein of SARS-CoV2 after 50 ns simulations. Red chains are conjugated peptides, grey chains are generation 4 PAMAM dendrimer, and blue chains are the RBD. (d) The free energy of binding between isolated and dendrimer-conjugated peptides and RBD. (e) The same as d) for RMSDs. Grey - isolated peptides, orange – dendrimer-conjugated

1  
2  
3 peptides, and blue - the entire peptide conjugated dendrimer and RBD complex. Note that MMGB-  
4  
5  
6  
7 SA free energy and RMSD were calculated over final 50 ns of simulation.  
8  
9  
10  
11  
12  
13

## 14 CONCLUSION 15 16 17

18 It has been more than two years since the COVID-19 pandemic strongly impacted our lives.  
19  
20  
21 Despite the rapid development of various therapeutic options for COVID-19, the clinical outcomes  
22  
23  
24 of these early COVID-19 therapeutics were mostly disappointing. In this study, a novel SARS-  
25  
26  
27 CoV-2 antagonist was designed by the development of a peptide sequence (pACE2) which  
28  
29  
30 incorporated two different peptide fragments obtained from ACE2 protein, followed by the  
31  
32  
33 conjugation of these peptides to hyperbranched PAMAM dendrimers, in order to utilize the  
34  
35  
36 dendrimer-mediated multivalent binding effect. The SPR measurements revealed the enhanced  
37  
38 binding interaction between pACE2 to SARS-CoV-2 spike proteins due to high generation  
39  
40  
41 PAMAM dendrimers. Specifically, the G7-pACE2 conjugates demonstrated three orders of  
42  
43  
44 magnitude stronger binding kinetics than the free pACE2, whereas the enhancement was only  
45  
46  
47  
48 12.8-fold for G4-pACE2. This clearly indicates that the dendrimer-mediated multivalent binding  
49  
50  
51 effect results in strong SARS-CoV-2 avidity. The *in vitro* assay using SARS-CoV-2-mimicking  
52  
53  
54  
55  
56  
57  
58  
59  
60

1  
2  
3 microbeads also demonstrated the effective blockade of binding between ACE2 and SARS-CoV-  
4  
5  
6 2 spike proteins for the dendrimer-pACE2 conjugates. The treatment of G4-pACE2 and G7-  
7  
8 pACE2 conjugates to the SARS-CoV-2-mimicking microbeads resulted in 39.3% and 51.4%  
9  
10 reduced binding to ACE2-positive MCF-7 cells, respectively. Furthermore, the interaction  
11  
12 between the newly developed DPCs and SARS-CoV-2 was simulated using the MD method,  
13  
14 providing an insight of how our DPC system enhances the SARS-CoV-2 blockade effect.  
15  
16  
17  
18  
19  
20  
21  
22  
23  
24

25 Some recent studies have demonstrated that SARS-CoV-2 may also infect tissues that do  
26  
27 not express ACE2.<sup>53</sup> This report suggested that there are other mechanisms involved for the entry  
28  
29 of SARS-CoV-2 other than the interaction between SARS-CoV-2-spike protein and ACE2  
30  
31 proteins. Although our study was focused on blocking the interactions between SARS-CoV-2  
32  
33  
34 Spike protein and ACE2 proteins, our DPC systems can be further employed for inhibiting other  
35  
36 receptors that may cause the entry of SARS-CoV-2 into cells. Previously, our team has shown that  
37  
38 the dendrimer-mediated multivalent binding effect can facilitate the targeting of multiple proteins  
39  
40  
41 on the cell surface by co-conjugating peptides that target different cell surface proteins on the  
42  
43  
44 dendrimer surface.<sup>38</sup> Thus, other types of peptides that inhibit the entry of virus to the cells may  
45  
46  
47 be co-immobilized on our DPC system, which has potential to further prevent the SARS-CoV-2  
48  
49  
50  
51  
52  
53  
54  
55  
56  
57  
58  
59  
60

1  
2  
3 infection. The therapeutic efficacy, bioavailability, and pharmacokinetics of our inhibitor will be  
4  
5 the subject of our future studies that will focus on their *in vivo* behaviors. Nevertheless, the results  
6  
7 presented in this study show that the dendrimer-mediated multivalent binding effect can enhance  
8  
9 the SARS-CoV-2 antagonist effect, providing a novel potential antiviral drug delivery system for  
10  
11 COVID-19, which could be potentially applied for other pandemic that may arise in the future.  
12  
13 Nevertheless, the results presented in this study show that the dendrimer-mediated multivalent  
14  
15 binding effect can enhance the SARS-CoV-2 antagonist effect, providing a novel potential  
16  
17 antiviral drug delivery system for COVID-19, which could be potentially applied for other  
18  
19 pandemic that may arise in the future.  
20  
21  
22  
23  
24  
25  
26  
27  
28  
29  
30  
31

32  
33  
34  
35  
36  
37  
38 ASSOCIATED CONTENT  
39  
40

41  
42  
43  
44 Supporting Information.  
45  
46  
47

48 The Supporting Information is available free of charge:  
49  
50  
51

52 MALDI-TOF MS, CD, HPLC, <sup>1</sup>H NMR, TEM, DLS, and SPR data  
53  
54  
55  
56  
57  
58  
59  
60

1  
2  
3  
4  
5  
6  
7  
**AUTHOR INFORMATION**  
8  
9  
1011  
12  
13  
14  
**Corresponding Authors**  
15  
16  
17  
18  
19  
20  
21  
22  
23

\*Prof. Seungpyo Hong; E-mail: seungpyo.hong@wisc.edu

\*Prof. Petr Kral; E-mail: pkral@uic.edu

\* Dr. Heejoo Hong; E-mail: hhong@amc.seoul.kr

24  
25  
26  
27  
**Author Contributions**  
28  
29  
30  
31  
32  
33  
34

The manuscript was written through contributions of all authors. All authors have given approval  
to the final version of the manuscript. ‡These authors contributed equally.

35  
36  
37  
38  
**Funding Sources**  
39  
40  
41  
42  
43  
44  
45  
46

This study was partially supported by National Science Foundation (NSF) under grant # DMR-1808251 and 2211932. The authors  
also acknowledge the partial support from the Wisconsin Head & Neck Cancer SPORE Grant from NIH (P50-DE026787), The  
Falk Medical Research Trust – Catalyst and Transformational Awards Program, and Milton J. Henrichs Chair Funds. Partial support  
from the National Research Foundation of Korea (NRF) grant funded by the Ministry of Science and ICT (2021R1C1C1009912,  
2021R1A4A3024237) is also acknowledged.

47  
48  
49  
**Notes**  
50  
51  
52

The authors declare no competing financial interest.

54  
55  
56  
57  
58  
59  
**REFERENCES**  
60

1  
2  
3 (1) Gao, G. F. From “A”IV to “Z”IKV: Attacks from Emerging and Re-Emerging Pathogens. *Cell*  
4 2018, 172(6), 1157–1159. <https://doi.org/10.1016/j.cell.2018.02.025>.

5  
6 (2) Zhu, N.; Zhang, D.; Wang, W.; Li, X.; Yang, B.; Song, J.; Zhao, X.; Huang, B.; Shi, W.; Lu,  
7 R.; Niu, P.; Zhan, F.; Ma, X.; Wang, D.; Xu, W.; Wu, G.; Gao, G. F.; Tan, W. A Novel  
8 Coronavirus from Patients with Pneumonia in China, 2019. *N. Engl. J. Med.* 2020, 382(8),  
9 727–733. <https://doi.org/10.1056/NEJMoa2001017>.

10  
11 (3) Su, S.; Wong, G.; Shi, W.; Liu, J.; Lai, A. C. K.; Zhou, J.; Liu, W.; Bi, Y.; Gao, G. F.  
12 Epidemiology, Genetic Recombination, and Pathogenesis of Coronaviruses. *Trends  
13 Microbiol.* 2016, 24(6), 490–502. <https://doi.org/10.1016/j.tim.2016.03.003>.

14  
15 (4) Zaki, A. M.; van Boheemen, S.; Bestebroer, T. M.; Osterhaus, A. D. M. E.; Fouchier, R. A.  
16 M. Isolation of a Novel Coronavirus from a Man with Pneumonia in Saudi Arabia. *N. Engl.  
17 J. Med.* 2012, 367(19), 1814–1820. <https://doi.org/10.1056/NEJMoa1211721>.

18  
19 (5) Cui, J.; Li, F.; Shi, Z.-L. Origin and Evolution of Pathogenic Coronaviruses. *Nat. Rev.  
20 Microbiol.* 2019, 17(3), 181–192. <https://doi.org/10.1038/s41579-018-0118-9>.

21  
22 (6) Gorbalya, A. E.; Baker, S. C.; Baric, R. S.; de Groot, R. J.; Drosten, C.; Gulyaeva, A. A.;  
23 Haagmans, B. L.; Lauber, C.; Leontovich, A. M.; Neuman, B. W.; Penzar, D.; Perlman, S.;  
24 Poon, L. L. M.; Samborskiy, D. V.; Sidorov, I. A.; Sola, I.; Ziebuhr, J.; Coronaviridae Study  
25 Group of the International Committee on Taxonomy of Viruses. The Species Severe Acute  
26 Respiratory Syndrome-Related Coronavirus%: Classifying 2019-NCoV and Naming It  
27 SARS-CoV-2. *Nat. Microbiol.* 2020, 5 (4), 536–544. <https://doi.org/10.1038/s41564-020-0695-z>.

28  
29 (7) Lu, R.; Zhao, X.; Li, J.; Niu, P.; Yang, B.; Wu, H.; Wang, W.; Song, H.; Huang, B.; Zhu, N.;  
30 Bi, Y.; Ma, X.; Zhan, F.; Wang, L.; Hu, T.; Zhou, H.; Hu, Z.; Zhou, W.; Zhao, L.; Chen, J.;  
31 Meng, Y.; Wang, J.; Lin, Y.; Yuan, J.; Xie, Z.; Ma, J.; Liu, W. J.; Wang, D.; Xu, W.; Holmes,  
32 E. C.; Gao, G. F.; Wu, G.; Chen, W.; Shi, W.; Tan, W. Genomic Characterisation and Receptor  
33 Binding. *Lancet* 2020, 395 (10224), 565–574. [https://doi.org/10.1016/S0140-6736\(20\)30251-8](https://doi.org/10.1016/S0140-6736(20)30251-8).

34  
35  
36  
37  
38  
39  
40  
41  
42  
43  
44  
45  
46  
47  
48  
49  
50  
51  
52  
53  
54  
55  
56  
57  
58  
59  
60

1  
2  
3 (8) Guan, W.; Ni, Z.; Hu, Y.; Liang, W.; Ou, C.; He, J.; Liu, L.; Shan, H.; Lei, C.; Hui, D. S. C.;  
4 Du, B.; Li, L.; Zeng, G.; Yuen, K.-Y.; Chen, R.; Tang, C.; Wang, T.; Chen, P.; Xiang, J.; Li,  
5 S.; Wang, J.; Liang, Z.; Peng, Y.; Wei, L.; Liu, Y.; Hu, Y.; Peng, P.; Wang, J.; Liu, J.; Chen,  
6 Z.; Li, G.; Zheng, Z.; Qiu, S.; Luo, J.; Ye, C.; Zhu, S.; Zhong, N. Clinical Characteristics of  
7 Coronavirus Disease 2019 in China. *N. Engl. J. Med.* **2020**, *382* (18), 1708–1720.  
8 <https://doi.org/10.1056/NEJMoa2002032>.  
9  
10 (9) Cucinotta, D.; Vanelli, M. WHO Declares COVID-19 a Pandemic. *Acta Biomed.* **2020**, *91* (1),  
11 157–160. <https://doi.org/10.23750/abm.v91i1.9397>.  
12  
13 (10) Kerr, C. C.; Mistry, D.; Stuart, R. M.; Rosenfeld, K.; Hart, G. R.; Núñez, R. C.; Cohen, J. A.;  
14 Selvaraj, P.; Abeysuriya, R. G.; Jastrzebski, M.; George, L.; Hagedorn, B.; Panovska-  
15 Griffiths, J.; Fagalde, M.; Duchin, J.; Famulare, M.; Klein, D. J. Controlling COVID-19 via  
16 Test-Trace-Quarantine. *Nat. Commun.* **2021**, *12* (1), 2993. <https://doi.org/10.1038/s41467-021-23276-9>.  
17  
18 (11) Mathieu, E.; Ritchie, H.; Ortiz-Ospina, E.; Roser, M.; Hasell, J.; Appel, C.; Giattino, C.;  
19 Rodés-Guirao, L. A Global Database of COVID-19 Vaccinations. *Nature Human Behaviour*  
20 2021, 1–7. <https://doi.org/10.1038/s41562-021-01122-8>.  
21  
22 (12) Dong, E.; Du, H.; Gardner, L. An Interactive Web-Based Dashboard to Track COVID-19 in  
23 Real Time. *Lancet Infect. Dis.* **2020**, *20* (5), 533–534. [https://doi.org/10.1016/S1473-3099\(20\)30120-1](https://doi.org/10.1016/S1473-3099(20)30120-1).  
24  
25 (13) Han, Y.; Král, P. Computational Design of ACE2-Based Peptide Inhibitors of SARS-CoV-2.  
26 *ACS Nano* **2020**, *14* (4), 5143–5147. <https://doi.org/10.1021/acsnano.0c02857>.  
27  
28 (14) Chaturvedi, P.; Han, Y.; Král, P.; Vuković, L. Adaptive Evolution of Peptide Inhibitors for  
29 Mutating SARS-CoV-2. *Adv. Theory Simul.* **2020**, *3* (12), 2000156.  
30 <https://doi.org/10.1002/adts.202000156>.  
31  
32 (15) Wells, L.; Vierra, C.; Hardman, J.; Han, Y.; Dimas, D.; Gwarada-Phillips, L. N.; Blackeye,  
33 R.; Eggers, D. K.; LaBranche, C. C.; Král, P.; McReynolds, K. D. Sulfoglycodendrimer  
34 Therapeutics for HIV-1 and SARS-CoV-2. *Adv Ther (Weinh)*. **2021**, *4* (4), 2000210.  
35 <https://doi.org/10.1002/adtp.202000210>.  
36  
37  
38  
39  
40  
41  
42  
43  
44  
45  
46  
47  
48  
49  
50  
51  
52  
53  
54  
55  
56  
57  
58  
59  
60

1  
2  
3 (16) Gavriatopoulou, M.; Ntanasis-Stathopoulos, I.; Korompoki, E.; Fotiou, D.; Migkou, M.;  
4 Tzanninis, I.-G.; Psaltopoulou, T.; Kastritis, E.; Terpos, E.; Dimopoulos, M. A. Emerging  
5 Treatment Strategies for COVID-19 Infection. *Clin. Exp. Med.* **2021**, *21* (2), 167–179.  
6 <https://doi.org/10.1007/s10238-020-00671-y>.  
7  
8 (17) Le Bras, A. Efficacy of Remdesivir in a Rhesus Macaque Model of MERS-CoV Infection.  
9 *Lab. Anim.* **2020**, *49* (5), 150–150. <https://doi.org/10.1038/s41684-020-0537-x>.  
10  
11 (18) Sheahan, T. P.; Sims, A. C.; Leist, S. R.; Schäfer, A.; Won, J.; Brown, A. J.; Montgomery,  
12 S. A.; Hogg, A.; Babusis, D.; Clarke, M. O.; Spahn, J. E.; Bauer, L.; Sellers, S.; Porter, D.;  
13 Feng, J. Y.; Cihlar, T.; Jordan, R.; Denison, M. R.; Baric, R. S. Comparative Therapeutic  
14 Efficacy of Remdesivir and Combination Lopinavir, Ritonavir, and Interferon Beta against  
15 MERS-CoV. *Nat. Commun.* **2020**, *11* (1), 222. <https://doi.org/10.1038/s41467-019-13940-6>.  
16  
17 (19) Repurposed Antiviral Drugs for Covid-19 — Interim WHO Solidarity Trial Results. *N. Engl.  
18 J. Med.* **2021**, *384* (6), 497–511. <https://doi.org/10.1056/NEJMoa2023184>.  
19  
20 (20) Bosilkovski, M.; Jakimovski, D.; Poposki, K.; Mateska, S.; Grujoski, M.; Dimzova, M.  
21 CURRENT SITUATION IN CHEMOPROPHYLAXIS AND THERAPEUTIC  
22 TREATMENT OF COVID-19. *Academic Medical Journal* **2022**, *2* (1), 4–12.  
23 <https://doi.org/10.53582/AMJ2221004b>.  
24  
25 (21) Wu, Y.; Wang, F.; Shen, C.; Peng, W.; Li, D.; Zhao, C.; Li, Z.; Li, S.; Bi, Y.; Yang, Y.; Gong,  
26 Y.; Xiao, H.; Fan, Z.; Tan, S.; Wu, G.; Tan, W.; Lu, X.; Fan, C.; Wang, Q.; Liu, Y.; Zhang,  
27 C.; Qi, J.; Gao, G. F.; Gao, F.; Liu, L. A Noncompeting Pair of Human Neutralizing  
28 Antibodies Block COVID-19 Virus Binding to Its Receptor ACE2. *Sci.* **2020**, *368* (6496),  
29 1274–1278. <https://doi.org/10.1126/science.abc2241>.  
30  
31 (22) Letko, M.; Marzi, A.; Munster, V. Functional Assessment of Cell Entry and Receptor Usage  
32 for SARS-CoV-2 and Other Lineage B Betacoronaviruses. *Nat. Microbiol.* **2020**, *5* (4), 562–  
33 569. <https://doi.org/10.1038/s41564-020-0688-y>.  
34  
35 (23) Surnar, B.; Kamran, M. Z.; Shah, A. S.; Dhar, S. Clinically Approved Antiviral Drug in an  
36 Orally Administrable Nanoparticle for COVID-19. *ACS Pharmacol. Transl. Sci.* **2020**, *3* (6),  
37 1371–1380. <https://doi.org/10.1021/acsptsci.0c00179>.  
38  
39  
40  
41  
42  
43  
44  
45  
46  
47  
48  
49  
50  
51  
52  
53  
54  
55  
56  
57  
58  
59  
60

1  
2  
3  
4 (24) Wrapp, D.; Wang, N.; Corbett, K. S.; Goldsmith, J. A.; Hsieh, C.-L.; Abiona, O.; Graham,  
5 B. S.; McLellan, J. S. Cryo-EM Structure of the 2019-NCoV Spike in the Prefusion  
6 Conformation. *bioRxiv* 2020, 2020.02.11.944462.  
7  
8 <https://doi.org/10.1101/2020.02.11.944462>.

9  
10  
11 (25) Lan, J.; Ge, J.; Yu, J.; Shan, S.; Zhou, H.; Fan, S.; Zhang, Q.; Shi, X.; Wang, Q.; Zhang, L.;  
12 Wang, X. Structure of the SARS-CoV-2 Spike Receptor-Binding Domain Bound to the  
13 ACE2 Receptor. *Nat.* 2020, 581 (7807), 215–220. <https://doi.org/10.1038/s41586-020-2180-5>.

14  
15  
16  
17  
18 (26) Huang, K.-W.; Hsu, F.-F.; Qiu, J. T.; Chern, G.-J.; Lee, Y.-A.; Chang, C.-C.; Huang, Y.-T.;  
19 Sung, Y.-C.; Chiang, C.-C.; Huang, R.-L.; Lin, C.-C.; Dinh, T. K.; Huang, H.-C.; Shih, Y.-  
20 C.; Alson, D.; Lin, C.-Y.; Lin, Y.-C.; Chang, P.-C.; Lin, S.-Y.; Chen, Y. Highly Efficient and  
21 Tumor-Selective Nanoparticles for Dual-Targeted Immunogene Therapy against Cancer. *Sci.*  
22 *Adv.* 2020, 6 (3), eaax5032. <https://doi.org/10.1126/sciadv.aax5032>.

23  
24  
25  
26 (27) Xia, S.; Zhu, Y.; Liu, M.; Lan, Q.; Xu, W.; Wu, Y.; Ying, T.; Liu, S.; Shi, Z.; Jiang, S.; Lu,  
27 L. Fusion Mechanism of 2019-NCoV and Fusion Inhibitors Targeting HR1 Domain in Spike  
28 Protein. *Cell. Mol. Immunol.* 2020, 17 (7), 765–767. <https://doi.org/10.1038/s41423-020-0374-2>.

29  
30  
31  
32 (28) Robbiani, D. F.; Gaebler, C.; Muecksch, F.; Lorenzi, J. C. C.; Wang, Z.; Cho, A.; Agudelo,  
33 M.; Barnes, C. O.; Gazumyan, A.; Finkin, S.; Hagglof, T.; Oliveira, T. Y.; Viant, C.; Hurley,  
34 A.; Hoffmann, H.-H.; Millard, K. G.; Kost, R. G.; Cipolla, M.; Gordon, K.; Bianchini, F.;  
35 Chen, S. T.; Ramos, V.; Patel, R.; Dizon, J.; Shimeliovich, I.; Mendoza, P.; Hartweger, H.;  
36 Nogueira, L.; Pack, M.; Horowitz, J.; Schmidt, F.; Weisblum, Y.; Michailidis, E.; Ashbrook,  
37 A. W.; Waltari, E.; Pak, J. E.; Huey-Tubman, K. E.; Koranda, N.; Hoffman, P. R.; West, A.  
38 P.; Rice, C. M.; Hatzioannou, T.; Bjorkman, P. J.; Bieniasz, P. D.; Caskey, M.; Nussenzweig,  
39 M. C. Convergent Antibody Responses to SARS-CoV-2 Infection in Convalescent  
40 Individuals; preprint; *Immunol.*, 2020. <https://doi.org/10.1101/2020.05.13.092619>.

41  
42  
43  
44 (29) Shi, R.; Shan, C.; Duan, X.; Chen, Z.; Liu, P.; Song, J.; Song, T.; Bi, X.; Han, C.; Wu, L.;  
45 Gao, G.; Hu, X.; Zhang, Y.; Tong, Z.; Huang, W.; Liu, W. J.; Wu, G.; Zhang, B.; Wang, L.;  
46 Qi, J.; Feng, H.; Wang, F.-S.; Wang, Q.; Gao, G. F.; Yuan, Z.; Yan, J. A Human Neutralizing  
47  
48  
49  
50  
51  
52  
53  
54  
55  
56  
57  
58  
59  
60

1  
2  
3 Antibody Targets the Receptor-Binding Site of SARS-CoV-2. *Nat.* **2020**, *584* (7819), 120–  
4 124. <https://doi.org/10.1038/s41586-020-2381-y>.

5  
6  
7 (30) Chen, P.; Nirula, A.; Heller, B.; Gottlieb, R. L.; Boscia, J.; Morris, J.; Huhn, G.; Cardona, J.;  
8 Mocherla, B.; Stosor, V.; Shawa, I.; Adams, A. C.; Van Naarden, J.; Custer, K. L.; Shen, L.;  
9 Durante, M.; Oakley, G.; Schade, A. E.; Sabo, J.; Patel, D. R.; Klekotka, P.; Skovronsky, D.  
10 M. SARS-CoV-2 Neutralizing Antibody LY-CoV555 in Outpatients with Covid-19. *N. Engl.  
11 J. Med.* **2021**, *384* (3), 229–237. <https://doi.org/10.1056/NEJMoa2029849>.

12  
13  
14  
15  
16 (31) Weinreich, D. M.; Sivapalasingam, S.; Norton, T.; Ali, S.; Gao, H.; Bhore, R.; Musser, B. J.;  
17 Soo, Y.; Rofail, D.; Im, J.; Perry, C.; Pan, C.; Hosain, R.; Mahmood, A.; Davis, J. D.; Turner,  
18 K. C.; Hooper, A. T.; Hamilton, J. D.; Baum, A.; Kyratsous, C. A.; Kim, Y.; Cook, A.;  
19 Kampman, W.; Kohli, A.; Sachdeva, Y.; Graber, X.; Kowal, B.; DiCioccio, T.; Stahl, N.;  
20 Lipsich, L.; Braunstein, N.; Herman, G.; Yancopoulos, G. D. REGN-COV2, a Neutralizing  
21 Antibody Cocktail, in Outpatients with Covid-19. *N. Engl. J. Med.* **2021**, *384* (3), 238–251.  
22 <https://doi.org/10.1056/NEJMoa2035002>.

23  
24  
25  
26  
27  
28 (32) Pardi, N.; Weissman, D. Development of Vaccines and Antivirals for Combating Viral  
29 Pandemics. *Nat. Biomed. Eng.* **2020**, *4* (12), 1128–1133. <https://doi.org/10.1038/s41551-020-00658-w>.

30  
31  
32 (33) Sun, Y.; Ho, M. Emerging Antibody-Based Therapeutics against SARS-CoV-2 during the  
33 Global Pandemic. *Antibody Ther.* **2020**, *3* (4), 246–256. <https://doi.org/10.1093/abt/tbaa025>.

34  
35  
36 (34) Salian, V. S.; Wright, J. A.; Vedell, P. T.; Nair, S.; Li, C.; Kandimalla, M.; Tang, X.; Carmona  
37 Porquera, E. M.; Kalari, K. R.; Kandimalla, K. K. COVID-19 Transmission, Current  
38 Treatment, and Future Therapeutic Strategies. *Mol. Pharmaceutics* **2021**, *18* (3), 754–771.  
39 <https://doi.org/10.1021/acs.molpharmaceut.0c00608>.

40  
41  
42 (35) Pomplun, S.; Jbara, M.; Quartararo, A. J.; Zhang, G.; Brown, J. S.; Lee, Y.-C.; Ye, X.; Hanna,  
43 S.; Pentelute, B. L. De Novo Discovery of High-Affinity Peptide Binders for the SARS-CoV-  
44 2 Spike Protein. *ACS Cent. Sci.* **2021**, *7* (1), 156–163.  
45 <https://doi.org/10.1021/acscentsci.0c01309>.

46  
47  
48  
49  
50  
51  
52  
53  
54  
55  
56  
57  
58  
59  
60

1  
2  
3  
4  
5  
6  
7  
8  
9  
10  
11  
12  
13  
14  
15  
16  
17  
18  
19  
20  
21  
22  
23  
24  
25  
26  
27  
28  
29  
30  
31  
32  
33  
34  
35  
36  
37  
38  
39  
40  
41  
42  
43  
44  
45  
46  
47  
48  
49  
50  
51  
52  
53  
54  
55  
56  
57  
58  
59  
60

(36) Jeong, W.-J.; Bu, J.; Han, Y.; Drelich, A. J.; Nair, A.; Král, P.; Hong, S. Nanoparticle Conjugation Stabilizes and Multimerizes  $\beta$ -Hairpin Peptides To Effectively Target PD-1/PD-L1  $\beta$ -Sheet-Rich Interfaces. *J. Am. Chem. Soc.* **2020**, *142* (4), 1832–1837. <https://doi.org/10.1021/jacs.9b10160>.

(37) Lau, J. L.; Dunn, M. K. Therapeutic Peptides: Historical Perspectives, Current Development Trends, and Future Directions. *Bioorg. Med. Chem.* **2018**, *26* (10), 2700–2707. <https://doi.org/10.1016/j.bmc.2017.06.052>.

(38) Jeong, W.-J.; Bu, J.; Jafari, R.; Rehak, P.; Kubiatowicz, L. J.; Drelich, A. J.; Owen, R. H.; Nair, A.; Rawding, P. A.; Poellmann, M. J.; Hopkins, C. M.; Král, P.; Hong, S. Hierarchically Multivalent Peptide-Nanoparticle Architectures: A Systematic Approach to Engineer Surface Adhesion. *Adv Sci (Weinh)*. **2022**, *9*(4), e2103098. <https://doi.org/10.1002/advs.202103098>.

(39) Phillips, J. C.; Hardy, D. J.; Maia, J. D. C.; Stone, J. E.; Ribeiro, J. V.; Bernardi, R. C.; Buch, R.; Fiorin, G.; Hénin, J.; Jiang, W.; McGreevy, R.; Melo, M. C. R.; Radak, B. K.; Skeel, R. D.; Singharoy, A.; Wang, Y.; Roux, B.; Aksimentiev, A.; Luthey-Schulten, Z.; Kalé, L. V.; Schulten, K.; Chipot, C.; Tajkhorshid, E. Scalable Molecular Dynamics on CPU and GPU Architectures with NAMD. *J. Chem. Phys.* **2020**, *153* (4), 044130. <https://doi.org/10.1063/5.0014475>.

(40) Phillips, J. C.; Braun, R.; Wang, W.; Gumbart, J.; Tajkhorshid, E.; Villa, E.; Chipot, C.; Skeel, R. D.; Kalé, L.; Schulten, K. Scalable Molecular Dynamics with NAMD. *J. Comput. Chem.* **2005**, *26*(16), 1781–1802. <https://doi.org/10.1002/jcc.20289>.

(41) Brooks, B. R.; Brooks, C. L.; Mackerell, A. D.; Nilsson, L.; Petrella, R. J.; Roux, B.; Won, Y.; Archontis, G.; Bartels, C.; Boresch, S.; Caflisch, A.; Caves, L.; Cui, Q.; Dinner, A. R.; Feig, M.; Fischer, S.; Gao, J.; Hodoscek, M.; Im, W.; Kuczera, K.; Lazaridis, T.; Ma, J.; Ovchinnikov, V.; Paci, E.; Pastor, R. W.; Post, C. B.; Pu, J. Z.; Schaefer, M.; Tidor, B.; Venable, R. M.; Woodcock, H. L.; Wu, X.; Yang, W.; York, D. M.; Karplus, M. CHARMM: The Biomolecular Simulation Program. *J. Comput. Chem.* **2009**, *30* (10), 1545–1614. <https://doi.org/10.1002/jcc.21287>.

1  
2  
3 (42) Vanommeslaeghe, K.; Hatcher, E.; Acharya, C.; Kundu, S.; Zhong, S.; Shim, J.; Darian, E.;  
4 Guvench, O.; Lopes, P.; Vorobyov, I.; MacKerell, A. D. CHARMM General Force Field: A  
5 Force Field for Drug-like Molecules Compatible with the CHARMM All-Atom Additive  
6 Biological Force Fields. *J. Comput. Chem.* **2009**, NA-NA. <https://doi.org/10.1002/jcc.21367>.  
7  
8 (43) Yu, W.; He, X.; Vanommeslaeghe, K.; MacKerell, A. D. Extension of the CHARMM  
9 General Force Field to Sulfonyl-Containing Compounds and Its Utility in Biomolecular  
10 Simulations. *J. Comput. Chem.* **2012**, *33*(31), 2451–2468. <https://doi.org/10.1002/jcc.23067>.  
11  
12 (44) Darden, T.; York, D.; Pedersen, L. Particle Mesh Ewald: An N·log(N) Method for Ewald  
13 Sums in Large Systems. *J. Chem. Phys.* **1993**, *98* (12), 10089–10092.  
14 <https://doi.org/10.1063/1.464397>.  
15  
16 (45) Homeyer, N.; Gohlke, H. Free Energy Calculations by the Molecular Mechanics  
17 Poisson–Boltzmann Surface Area Method. *Mol. Inf.* **2012**, *31* (2), 114–122.  
18 <https://doi.org/10.1002/minf.201100135>.  
19  
20 (46) Vergara-Jaque, A.; Comer, J.; Monsalve, L.; González-Nilo, F. D.; Sandoval, C.  
21 Computationally Efficient Methodology for Atomic-Level Characterization of Dendrimer–  
22 Drug Complexes: A Comparison of Amine- and Acetyl-Terminated PAMAM. *J. Phys.*  
23 *Chem. B* **2013**, *117*(22), 6801–6813. <https://doi.org/10.1021/jp4000363>.  
24  
25 (47) Tanner, D. E.; Chan, K.-Y.; Phillips, J. C.; Schulten, K. Parallel Generalized Born Implicit  
26 Solvent Calculations with NAMD. *J. Chem. Theory Comput.* **2011**, *7*(11), 3635–3642.  
27 <https://doi.org/10.1021/ct200563j>.  
28  
29 (48) Han, Y.; McReynolds, K. D.; Kral, P. Retrained Generic Antibodies Can Recognize SARS-  
30 CoV-2. *ChemRxiv* **2020**, Preprint, 5. <https://doi.org/10.26434/chemrxiv.13249559.v1>.  
31  
32 (49) Jeong, W.-J.; Bu, J.; Han, Y.; Drelich, A. J.; Nair, A.; Král, P.; Hong, S. Nanoparticle  
33 Conjugation Stabilizes and Multimerizes  $\beta$ -Hairpin Peptides To Effectively Target PD-1/PD-  
34 L1  $\beta$ -Sheet-Rich Interfaces. *J. Am. Chem. Soc.* **2020**, *142* (4), 1832–1837.  
35 <https://doi.org/10.1021/jacs.9b10160>.  
36  
37  
38  
39  
40  
41  
42  
43  
44  
45  
46  
47  
48  
49  
50  
51  
52  
53  
54  
55  
56  
57  
58  
59  
60

1  
2  
3 (50) Jeong, W.; Choi, S.-H.; Jin, K. S.; Lim, Y. Tuning Oligovalent Biomacromolecular Interfaces  
4 Using Double-Layered  $\alpha$ -Helical Coiled-Coil Nanoassemblies from Lariat-Type Building  
5 Blocks. *ACS Macro Lett.* 2016, 5 (12), 1406–1410.  
6 <https://doi.org/10.1021/acsmacrolett.6b00746>.

7  
8 (51) Kim, J.-Y.; Lee, J. Y.; Park, H. Y.; Kim, H.; Kang, J. H.; Kim, H. J.; Jeong, W.-J.  
9 Combination of Peptides with Biological, Organic, and Inorganic Materials for  
10 Synergistically Enhanced Diagnostics and Therapeutics. *Pept. Sci.* 2022, 114 (3), e24233.  
11 <https://doi.org/10.1002/pep2.24233>.

12  
13 (52) Sen, S.; Han, Y.; Rehak, P.; Vuković, L.; Král, P. Computational Studies of Micellar and  
14 Nanoparticle Nanomedicines. *Chem. Soc. Rev.* 2018, 47 (11), 3849–3860.  
15 <https://doi.org/10.1039/C8CS00022K>.

16  
17 (53) Puray-Chavez, M.; LaPak, K. M.; Schrank, T. P.; Elliott, J. L.; Bhatt, D. P.; Agajanian, M.  
18 J.; Jasuja, R.; Lawson, D. Q.; Davis, K.; Rothlauf, P. W.; Liu, Z.; Jo, H.; Lee, N.; Tenneti,  
19 K.; Eschbach, J. E.; Shema Mugisha, C.; Cousins, E. M.; Cloer, E. W.; Vuong, H. R.;  
20 VanBlargan, L. A.; Bailey, A. L.; Gilchuk, P.; Crowe, J. E.; Diamond, M. S.; Hayes, D. N.;  
21 Whelan, S. P. J.; Horani, A.; Brody, S. L.; Goldfarb, D.; Major, M. B.; Kutluay, S. B.  
22 Systematic Analysis of SARS-CoV-2 Infection of an ACE2-Negative Human Airway Cell.  
23 *Cell Rep* 2021, 36 (2), 109364. <https://doi.org/10.1016/j.celrep.2021.109364>.

24  
25  
26  
27  
28  
29  
30  
31  
32  
33  
34  
35  
36  
37  
38  
39  
40  
41  
42  
43  
44  
45  
46  
47  
48  
49  
50  
51  
52  
53  
54  
55  
56  
57  
58  
59  
60

## SYNOPSIS.

